MESH SIZE INFLUENCE OF THE CONCRETE SLAB FE MODEL EXPOSED TO IMPACT LOAD FOR VARIOUS MATERIAL MODELS

Daniel JINDRA[1], *Petr HRADIL*[1], *Jiří KALA*[1], *Petr KRÁL*[1,2]

[1]Institute of Structural Mechanics, Faculty of Civil Engineering, Brno University of Technology,
Veveří 331/95, 602 00 Brno, Czech Republic
[2]Faculty of Civil Engineering, VSB – Technical University of Ostrava,
Ludvíka Podéště 1875/17, 708 00 Ostrava-Poruba, Czech Republic

jindra.d@fce.vutbr.cz, hradil.p@fce.vutbr.cz, kala.j@fce.vutbr.cz, petr.kral@vsb.cz

DOI: 10.35181/tces-2020-0010

Abstract. *Numerical approach using the FEM has been used to model the behaviour of the reinforced concrete specimen subjected to the pressure blast wave. The concrete structure is a slab freely supported around the perimeter by a steel plate and a concrete base. A simplified 3D blast model has been used, which involves the pure Lagrangian approach of FEM. The analyses have been conducted using explicit solver. 3 different non-linear material models of concrete have been used to capture the concrete behaviour: CSCM (Continuous surface cap model), Schwer Murray continuous surface cap model, and JHC (Johnson-Holmquist-Cook) material model. Influences of various mesh sizes on the final results (crack patterns, vertical deflection, strain-time dependence) are being monitored, compared with physical experiment data and discussed.*

Keywords

Blast load, continuous surface cap material model, Schwer Murray cap model, Johnson-Holmquist-Cook model, discretization, explicit analysis, numerical nonlinear analysis, reinforced concrete slab.

1. Introduction

Concrete is one of the most widely used materials in the civil engineering. Structures with high level of reliability are required to withstand not only standard situation loads, but also need to retain its resistance while exposed to severe extreme loads, such as e.g. explosions [1] or impacts [2]. In these cases, advanced modelling methods and non-linear material models needs to be used, as e.g. by Neuberger et al, who investigated the response of plates subjected to spherical explosions [3] or by Králik, who modelled the Aircraft impact [4]. Behaviour of concrete is mathematically described by many different material models, each determined by various parameters. Different approaches in modelling, material models, discretization features and model settings are suitable for different loading situations.

Concrete structures exposed to blast loading have been modelled e.g. by Tai et al [5]; Zhao and Chen [1], [6]; Thiagarajan et al [7]; Dubec, Maňas, Štoller and Stonis [8]. In this study, closer focus on a mesh size influence using 3 different non-linear concrete material models is investigated.

1.1. Physical model

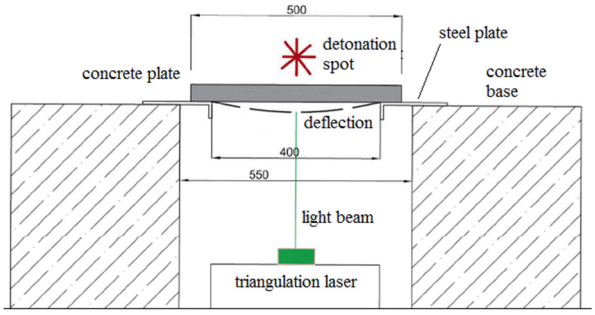

Fig. 1: Model geometry.

Fig. 2: Physical experiment set-up.

Physical experiments of the concrete slab specimen have been conducted and documented. In the height of 9 cm above the concrete slab centre, explosive of 75 g TNT has been placed (Fig. 1:). One specimen of the explosive in this distance has been tested.

The physical model geometry is depicted in the Fig. 1: Concrete slab is reinforced by a steel reinforcement bars Ø 6 á 100 mm in both perpendicular directions situated approximately in the middle of the slab height. Anchorage of the steel plate into the concrete base is provided by 4 bolts (in corners), and a rubber plate is located between the concrete base and the steel plate.

The objective of the measurement was to obtain stress-time curve (Fig. 3:). However in case of deflection-time dependence, only the maximal value of -3.8 mm is known to the author of this article.

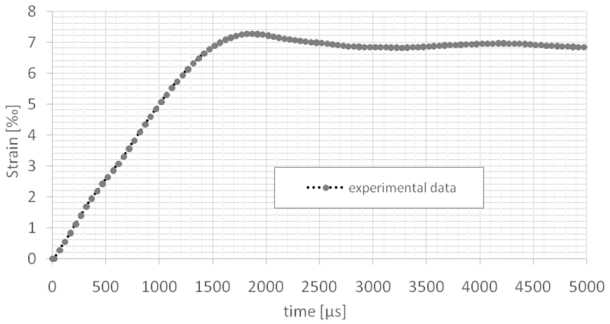

Fig. 3: Strain-time dependence based on experiment results.

1.2. Numerical model

A 3D numerical finite element model of the structure has been created in the environment of LS-Dyna [9], as the explicit approach of solving the equation of motion by a modification of the central difference time integration implemented in the solver of this software is suitable for analysing structures exposed to impact loading.

Hexahedron solid elements with reduced integration (1 point) have been used to model the concrete base, rubber (between the base and steel plate), and the test concrete slab. The maximal sizes of the rubber and concrete base elements are 25 mm and 50 mm respectively. The influence of the test concrete slab mesh size is one of the objectives of this study. In all cases, mesh consisting of regular hexahedral elements has been created, however with the different edge size of these elements: 7.5 mm, 5 mm, 2.5 mm or 1 mm.

Element size of the steel plate (15 mm thick) is the same as the size of concrete slab in area, where contact between these two parts occurs, getting coarser towards the edges (Fig. 4:). The steel plate has been modelled by shell elements with Belytschko-Tsay formulation and 2 integration points through the thickness. Beam elements with Hughes-Liu cross section integration and 2×2 Gauss quadrature beam integration rule have been used for the anchorage bolts and the reinforcement bars.

Symmetric contacts with segment based formulations (pinball algorithms) have been involved. These contacts have been defined between the concrete slab and the supporting steel plate (solid vs. shell element); between the steel plate and the rubber beneath it (shell vs. solid element), and between the rubber and the concrete base beneath it (solid vs. solid element).

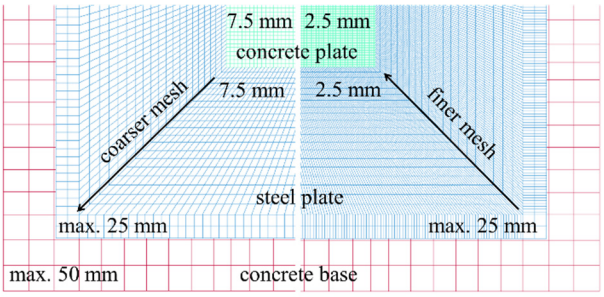

Fig. 4: Numerical model mesh geometry for various concrete slab mesh sizes (left 7.5 mm, right 2.5 mm) - top view.

1.3. Material models

1) Steel and rubber material

Both, reinforcement bars (also anchors) and support steel plate are considered by isotropic material model with plastic kinematic hardening. For these steel materials, elastic Young's modules of 200 and 210 GPa respectively have been used. Yield stresses of 500 and 235 MPa respectively have been defined. The rubber material between the steel plate and concrete base is considered as ideal elastic with elastic modulus of 5 MPa. Concrete density of 2200 kg·m^{-3} has been always considered.

2) Schwer Murray Cap model (MAT 145)

Schwer Murray material model [10] is based on a yield surface defined by the following function:

$$Y(I_1,J_2,J_3,\kappa) = J_2 - R(J_3)^2 F_f{}^2(I_1) F_c(I_1,\kappa)\,, \qquad (1)$$

where I_1 is the first invariant of the stress tensor. J_2 and J_3 are invariants of the deviatoric stress tensor. $R(J_3)$ is the Rubin strength reduction factor and κ is the cap hardening parameter. The yield surface consist of two parts: the hardening compaction surface $F_c(I_1,\kappa)$, and the shear failure surface $F_f(I_1)$, which is defined:

$$F_f(I_1) = \alpha - \lambda\, e^{-\beta I_1} + \theta I_1\,, \qquad (2)$$

where parameters α, β, λ and θ are determined by triaxial compression test results. The expression of the hardening compaction surface is defined by equations [11]:

$$F_c(I_1,\kappa) = 1 - \frac{(I_1 - L(\kappa))^2}{(X(\kappa) - L(\kappa))^2} \quad for\ I_1 > L(\kappa) \qquad (3)$$

$$F_c(I_1,\kappa) = 1 \quad for\ I_1 \le L(\kappa) \qquad (4)$$

$$L(\kappa) = \kappa \quad for\ \kappa > \kappa_0 \qquad (5)$$

$$L(\kappa) = \kappa_0 \quad for\ \kappa \le \kappa_0 \qquad (6)$$

$$X(\kappa) = L(\kappa) + R F_f(I_1)\,, \qquad (7)$$

where R is the cap aspect ratio. Hardening compaction surface and the shear failure surface are combined by a

multiplicative formulation which allows their continuous and smooth combination at their intersections.

Parameter values adopted for this material model are derived in accordance with study proposed by Jiang [12]. Uniaxial compression strength of concrete f_{cm} = 28 MPa (mean value of concrete class C20/25 [13]) has been considered for this process, and the derived values are depicted in the Fig. 5: below.

1	MID	RO	SHEAR	BULK	GRUN	SHOCK	PORE	
	1	2200.0000	1.250e+10	1.667e+10	0.0	0.0	1.0	
2	ALPHA	THETA	GAMMA	BETA	EFIT	FFIT	ALPHAN	CALPHA
	7.098e+06	0.3410000	2.681e+06	5.967e-08	1.0000000	0.0	0.0	0.0
3	RO	XO	IROCK	SECP	AFIT	BFIT	RDAMO	
	2.3460000	7.006e+07	1	0.0	1.0000000	1.809e-04	161.70000	
4	W	D1	D2	NPLOT	EPSMAX	CFIT	DFIT	TFAIL
	0.0650000	6.110e-10	2.225e-18	5.0000000	0.0	1.0000000	3.619e-04	2.200e+06
5	FAILFG	DBETA	DDELTA	VPTAU				
	1	0.0	0.0	0.0				
6	ALPHA1	THETA1	GAMMA1	BETA1	ALPHA2	THETA2	GAMMA2	BETA2
	8.300e+05	0.0	2.407e+05	1.398e-08	7.600e+05	0.0	2.600e+05	1.209e-08

Fig. 5: Material input card for MAT 145 (in SI units).

3) Continuous surface cap model (MAT 159)

Continuous surface cap material model is an updated version of the Schwer Murray cap model [9], [14], [15].

The parameters of this model have been documented e.g. by Král et al. [16]. In this case however, the default parameters suggested by Murray et al. [15] determined on the uniaxial compressive strength of 30 MPa and the maximal aggregate size of 8 mm has been used, and are summarized in the Fig. 6: below.

```
$#     mid        ro     nplot     incre     irate     erode     recov    itretrc
         1 2.200E+03         1 1.741E-05         1 0.000E+00 1.000E+00          0
$#     pre
 0.000E+00
$#       g         k     alpha     theta     lamda      beta        nh        ch
 1.146E+10 1.255E+10 1.450E+07 2.965E-01 1.051E+07 1.929E-08 1.000E+00 0.000E+00
$#  alpha1    theta1    lamda1     beta1    alpha2    theta2    lamda2     beta2
 7.473E-01 1.151E-09 1.700E-01 7.057E-08 6.600E-01 1.387E-09 1.600E-01 7.057E-08
$#       r        x0         w        d1        d2
 5.000E+00 9.054E+07 5.000E-02 2.500E-10 3.492E-19
$#       b       gfc         d       gft       gfs      pwrc      pwrt      pmod
 1.000E+02 5.392E+03 1.000E-01 5.392E+01 5.392E+01 5.000E+00 1.000E+00 0.000E+00
$#    eta0c        nc     eta0t        nt     overc     overt     srate     repow
 1.003E-04 7.800E-01 6.176E-05 4.800E-01 2.145E+07 2.145E+07 1.000E+00 1.000E+00
```

Fig. 6: Used parameter values for CSCM (in SI units).

4) Johnson-Holmquist-Cook (JHC) model

JHC material model is suitable to describe the mechanical behaviour of concrete constructions exposed to large strain rates [17].

The yield surface of JHC material model (Fig. 7:) considers the accumulated damage D ($0.0 \leq D \leq 1.0$) and is determined as:

$$\sigma^* = [A(1-D) + BP^{*N}]\,(1 + C\,ln\dot{\varepsilon}^*), \qquad (8)$$

where $P^*= P/f_c$ and $\sigma^*= \sigma/f_c$ are normalized equivalent pressure and stress respectively. P is the actual pressure and σ is the actual equivalent stress; f_c is the unconfined uniaxial compressive strength. The dimensionless strain rate is defined as $\dot{\varepsilon}^* = \varepsilon^*/\varepsilon_0{}^*$, where ε^* and $\varepsilon_0{}^*$ are actual and reference (*EPS0*) strain rates, respectively. Parameters A, B, C, N represents: normalized cohesive strength, normalized pressure hardening coefficient, strain rate coefficient and the pressure hardening exponent.

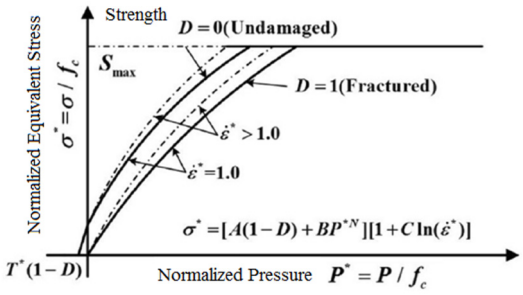

Fig. 7: Yield surface equation of JHC material model

Damage D (Fig. 8:) is accumulated from plastic strains. $\Delta\varepsilon_p$ is the effective plastic strain increment. $\Delta\mu_p$ is the plastic volumetric strain during a cycle of integration. Equation 9 defines the total plastic strain ${\varepsilon_p}^f + {\mu_p}^f$ under a constant pressure until fracture. D_1 and D_2 are the damage constants, and *EFMIN* is a material constant which suppress the fracture caused by weak tensile waves.

$$\varepsilon_p{}^f + \mu_p{}^f = D_1(P^* + T^*)^{D_2} \geq EFMIN \qquad (9)$$

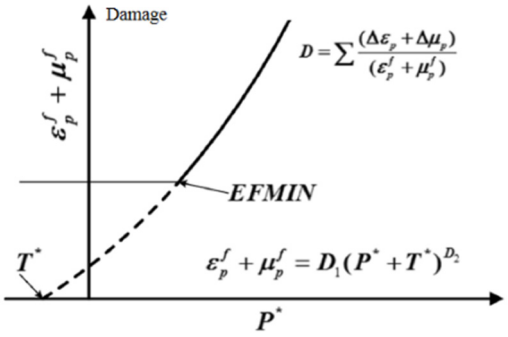

Fig. 8: JHC damage feature

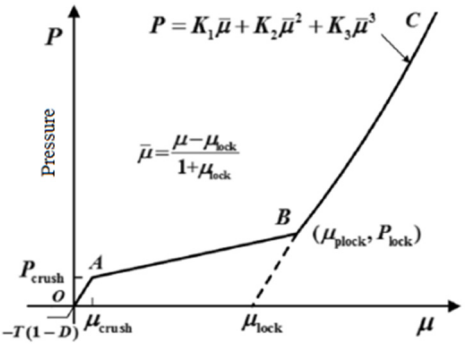

Fig. 9: Equation of state (EOS) of the JHC material model

The pressure-compaction response of the concrete is defined by equation of state (EOS), and is separated into three response phases (Fig. 9:). The first phase (0A) is considered as linear elastic between the negative pressure cut-off $-T(1-D)$ and the elastic limit value P_{crush}. The second phase (AB) is referred to the transitional region, where the air voids are compressed gradually out of the material and the plastic volumetric strain produces the compaction damage until reaching the value of μ_{lock}. The

third phase (BC) is defined as the compact region where all the air voids have been removed from the concrete material, and the behaviour is assumed non-linear elastic, defined by material constants K_1, K_2 and K_3.

Parameter values considered for this variant of material model are based on author's previous optimization process, and are summarized in paper [18].

1.4. Applied loads

The simplified blast model which involves the pure Lagrangian approach of FEM has been used. The blast wave is considered as a pressure load applied at the top surface of the concrete slab. The time dependence of pressure applied in a certain location (Eq. 10.) is based on the empirical blast loading functions by Randers-Pehrson and Bannister [19]. The blast loading equation is:

$$P(t) = P_r(t)\,cos^2\,\theta + P_s(t)(1 + cos^2\,\theta - 2cos\,\theta) \quad (10)$$

where θ is the angle of incidence (Fig. 10:). $P_r(t)$ and $P_s(t)$ are reflected and incident pressures (overpressures) respectively, both dependent on time t, and both defined by Friedlander equation (Eq. 11.) [20]. In case of $P_s(t)$, the function is stated as follows:

$$P_s(t) = P_{so}\left(1 - \frac{t}{t_o}\right) \cdot e^{-b\frac{t}{t_o}} \quad (11)$$

where P_{so} is the peak incident pressure, b is the waveform number and t_o is the positive phase duration. Parameters are defined in dependence on scaled distance Z, introduced by Hopkinson [21] and Cranz [22]:

$$Z = \frac{R}{W^{1/3}} \quad (12)$$

R is the distance from the centre of the blast, and W is the equivalent TNT mass. Parameters b and P_{so} (or P_r in case of peak reflected overpressure) are defined in a different way for incident and reflected overpressures. The values (in SI units) are obtained from JRC report [23], as well as the arrival time of the blast wave, t_A, (which is approx. 17 μs), and time t_o.

The incident and reflected overpressures for considered loading conditions are depicted in the Fig. 10:

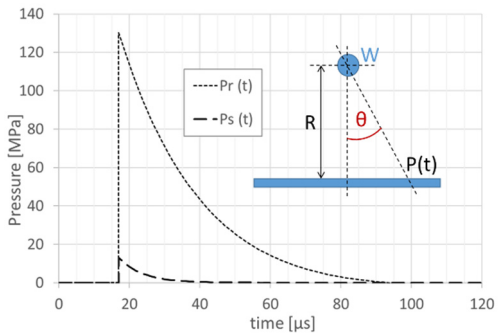

Fig. 10: Blast wave pressure load for W = 75 g and R = 9 cm.

No damping has been involved. The high speed phenomena is being modelled and involvement of the structural damping is rather useless [9].

2. Results

The analyses results are graphically depicted in the Fig. 11:. The legend is defined in Fig. 11: part e). The results are summarized for cases of 3 different material models, what is distinguished by a different curve colour (CSCM - blue; MAT145 - red; JHC - green). Also 4 different cases of concrete slab mesh size are documented, and a different line-pattern is used for each case (7.5 mm mesh = full line; 5 mm = dash-dot line; 2.5 mm = dashed line; 1 mm = dotted line). Altogether the results of 12 model cases (#1 - #12) are documented in this study. In some cases, there was more significant difference between the mid-span bottom surface strain in one direction (parallel to slab edge) and the strain in the perpendicular direction (x and y orthogonal directions). These strains are distinguished by adopting a darker or lighter variant of used colour for that certain model case. The noticeable difference in strains of these orthogonal directions is observed only in model cases #1 - #4 (CSCM material model) (Fig. 11: part b). In cases where the MAT145 or JHC material models have been used, the difference between x and y strain was very negligible (Fig. 11: parts c, d). The frequency of the measurement (50 μs) is determined by the points at the experimental data reference curve. The initiation of slope of this reference curve is established to be in match with the arrival time of the blast wave (17 μs) determined by the simplified blast model approach [23], as the arrival time has not been defined by the experiment.

Crack patterns at the bottom slab surface are depicted in the matter of the first principal strains (logarithmic) in the Fig. 12: for selected model cases (see the legend Fig. 11: e) in certain times (always 190 and 990 μs after the initiation of the blast).

Almost in all the model cases, 1 point integration has been adopted for the solid elements of the concrete slab, as is described in the chapter 1.2, except of the case #4 (CSCM material model with 1 mm mesh size), where full integration of solid elements of concrete slab has been used instead.

Another little difference in the methodology of the presented results is in case of the mid-span displacements (Fig. 11: part a). For model cases #5 - #12, the displacement is being monitored at the bottom surface of the concrete slab, as it is supposed to be. However for model cases where the CSCM material model has been adopted (#1 to #4), this displacement has been monitored at the upper surface of the concrete slab. The reason of this is the high level of plasticity and un-real mesh deformation in the area around the bottom surface mid-span of the concrete slab (where a certain „bump in a shape of little hill" at the planar surface has developed). The difference between the mid-span displacements monitored at the upper and the bottom surface of the concrete slab for the rest of modelled cases (#5 to #12) is negligible, so there is not a significant inconsistency in the monitored result data.

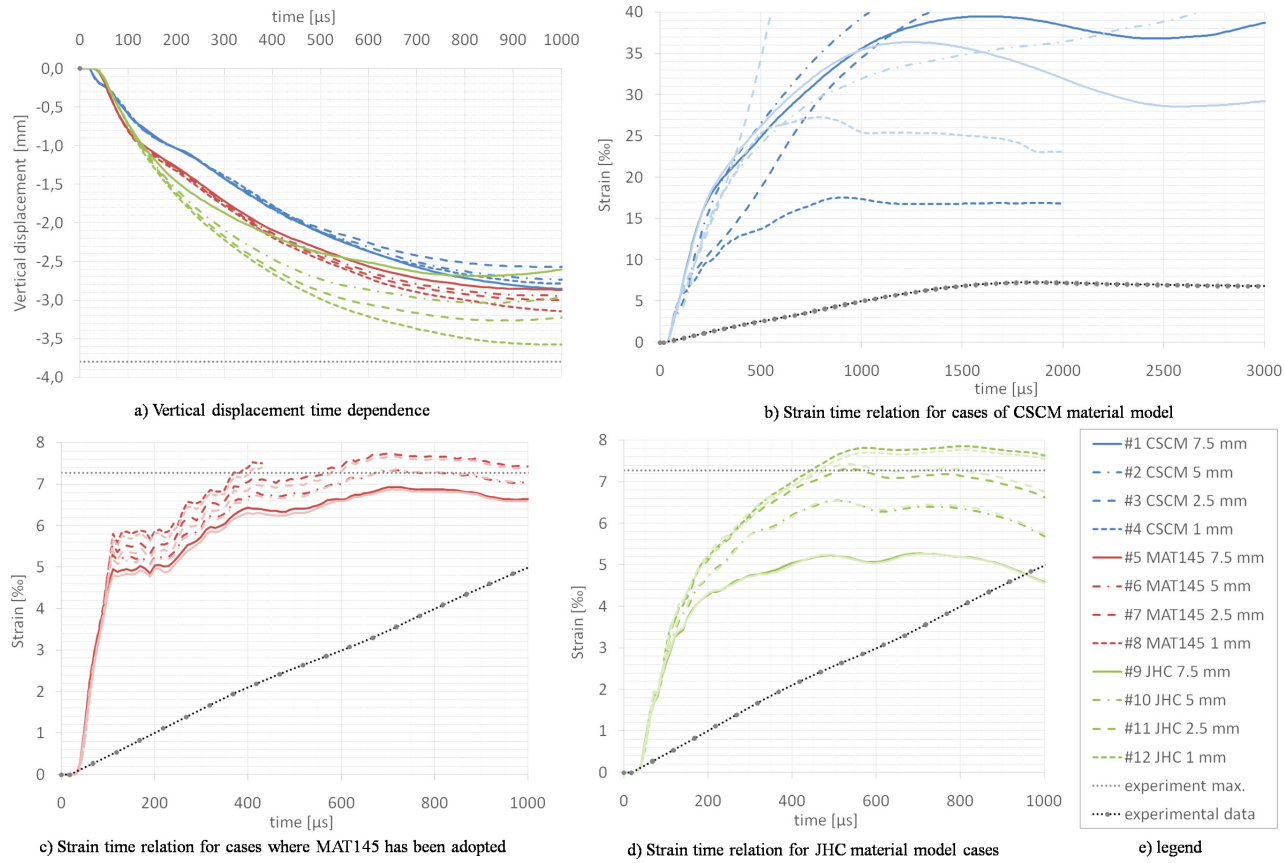

Fig. 11: Graphical results in time: a) Mid-span displacement; b) c) d) Mid-span bottom surface strains; e) Legend considering 4 various mesh sizes (7.5, 5, 2.5 and 1 mm) and 3 material models (CSCM, MAT145 and JHC); note: the darker and lighter colours of certain pattern (applicable for graphs b, c, d; noticeable difference only in b) determine two orthogonal directions (x and y) of strain for considered case.

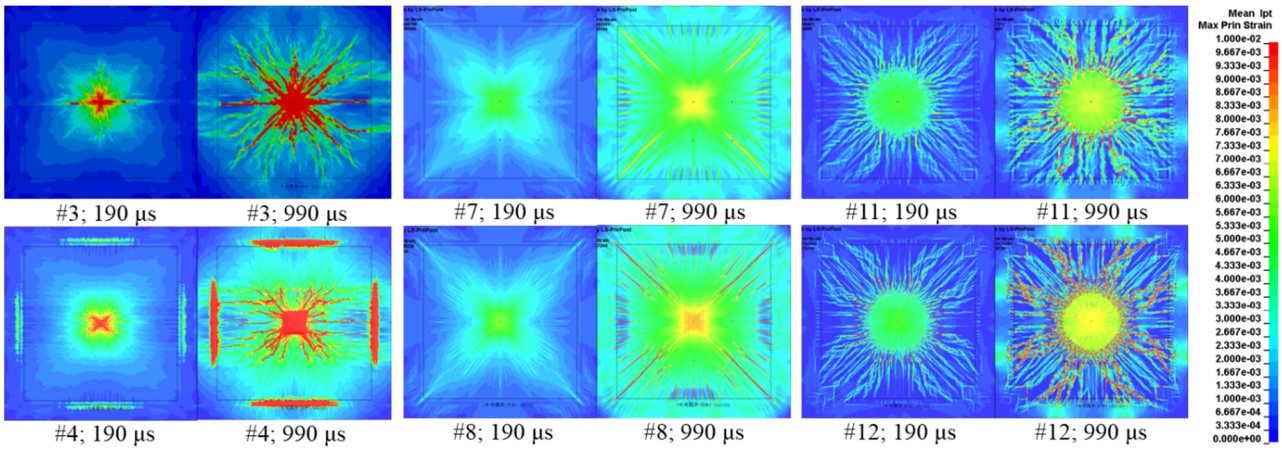

Fig. 12: 1st principal strain at the bottom slab surface for selected model cases (see the legend Fig. 11:e) in certain times.

3. Discussion

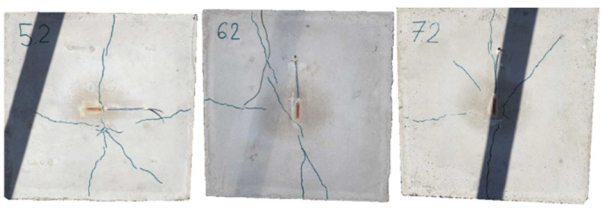

Fig. 13: Crack patterns of the slab after experiment (bottom surface).

In the matter of mid-span displacements (Fig. 11: part a), all the considered model cases resulted in a similar shape of displacement-time curve. For model cases where CSCM material model has been adopted (#1 to #4), there is no regular pattern observed. However for the other cases of material models, the finer mesh has been created, the larger is the displacement maximum, with more significant differences for the cases of the JHC material model (#9 to #12). All the displacement maximums are however slightly lower than the measured value of 3.8 mm, and ranges from 2.5 mm to 3.6 mm (for #12).

Crack patterns at the bottom surface of the concrete slab are depicted in the Fig. 13:. The TNT charge in the test specimens marked as 5.2 and 6.2 was in the distance of 10 cm from the upper slab surface, and in the variant 7.2 in the distance of 9 cm (as is considered for the numerical analyses). This difference is not so significant, however the strain-time experimental results were available only for the variant 7.2 (9 cm of TNT distance). The maximal mid-span displacements were similar in all the 3 variants, and the crack patterns are also very similar, forming in the directions diagonally as well as perpendicularly towards the slab edges.

The results of the CSCM material model cases (#1 to #4) have yielded in main crack patterns mostly in diagonal direction for coarser meshes. When sufficiently finer mesh has been adopted (Fig. 12: #3 #4) the crack formed also in a direction perpendicular to the slab edges. However in case of the mid-span strain monitored at the bottom surface (Fig. 11: b), there is a significant difference between two strains in mutually orthogonal directions (x, y), both perpendicular to the slab edges. Such difference is not expected in a symmetric model. Also significant difference not only in maximal values but also in global shape of the strain-time curve is being observed for various mesh sizes of the concrete slab. It is suitable to remind, that parameter values adopted for CSCM material model in this study were based only on rather robust (and automatized) determination implemented in LS-Dyna software [9], [14], [15]. It is not excluded that closer investigation of material parameters of this model would resulted in more reasonable data.

Model cases (#5 to #8) of the older version variant of CSCM material model, the Schwer-Murray material model (MAT 145), where the values of the material parameters have been determined more thoroughly, have yielded in more consistent results (Fig. 11: c). The difference between strains in two orthogonal directions is very negligible as expected. The strain maximum is increasing with finer mesh, however the global shape of the strain-time curve retains its shape. The maximal value of the strain is very close to the experimental value (7.2 ‰) for all the cases of the mesh size. However the slope of the strain-time curve is significantly steeper than the reference measurement. Also not even the finest mesh (1 mm) has yielded into crack patterns formed also in the perpendicular direction. All the main cracks close to the middle have been formed only in diagonal directions (Fig. 12: #7 and #8).

The results in the matter of strain-time dependences for cases of the JHC material model (Fig. 11: d) are very similar to the Schwer-Murray material model cases (Fig. 11: c). Similar patterns are being observed. In cases of JHC material model (#9 to #12) the concrete cracks are better developed also in the perpendicular direction (Fig. 12: #11 and #12). The initial slope of the strain-time dependence is however still much steeper than the experimental reference.

Overall a nice match between the displacement maximum and the experimental value is being observed. For model cases, where the concrete slab has been described by Schwer-Murray material model or the JHC material model (#5 to #12), also the maximal values of the strains monitored in the mid-span of the bottom surface are in a nice match with the experimental data. The effects of material, or perhaps also some geometric parameters, on the initial slope of the stress-time curve require further investigation.

Also it is suitable to mention, that the simplified blast approach considered in this study has a validity range of the scaled distance Z in the interval $\langle 0.147 ; 40 \rangle$ m·kg$^{-1/3}$ [9]. For 75 g of TNT in the distance of 9 cm, the scaled distance is equal to 0.213 m·kg$^{-1/3}$, what is pretty close to the edge of the interval. Therefore slightly different results might be also expected.

4. Conclusion

FE analyses of the concrete slab exposed to pressure wave after explosion of a TNT charge have been conducted. Three different material models have been adopted to describe the behaviour of the concrete slab exposed to the high velocity impact load. For each case, the effects of 4 different mesh sizes on the results have been investigated. The results are compared with experimental data. Maximal values of the mid-span displacement and strain, as well as the crack patterns are in a nice match with the reference data when suitable values of the material model parameters are adopted and sufficiently fine mesh is used. However the difference in the initial slope of the strain-time dependence between the experimental and the documented results requires further research.

Acknowledgements

This paper has been created with the financial support of the following projects: GAČR 17-23578S "Damage assessment identification for reinforced concrete subjected to extreme loading" provided by the Czech Science Foundation; FAST-J-20-6256 provided by the Brno University of Technology fund for the specific university research.

References

[1] ZHAO, C.F., J.Y. CHEN, Y. WANG and S.J. LU. Damage mechanism and response of reinforced concrete containment structure under internal blast loading. *Theoretical and Applied Fracture Mechanics*. 2012, vol. 61, p. 12-20. ISSN 0167-8442. DOI: 10.1016/j.tafmec.2012.08.002.

[2] FUJIKAKE, Kazunori, Bing LI a Sam SOEUN. Impact Response of Reinforced Concrete Beam and Its Analytical Evaluation. *In: Journal of Structural Engineering*. ASCE, 2009, 135(8), p. 938-950. ISSN: 0733-9445. DOI: 10.1061/(ASCE)ST.1943-541X.0000039.

[3] NEUBERGER, A., S. PELES and D. RITTEL. Scaling the response of circular plates subjected to large and close-range spherical explosions. Part I: Air-blast loading. *International Journal of Impact Engineering*. 2007, vol. 34, is. 5, p. 859-873. ISSN 0734-743X. DOI: 10.1016/j.ijimpeng.2006.04.001.

[4] KRÁLIK, J., Safety of nuclear power plant against the aircraft attack. *Applied Mechanics and Materials*. 2014, vol. 617, p. 76-80. ISSN: 1662−7482. DOI: 10.4028/www.scientific.net/AMM.617.76.

[5] TAI, Y.S., T.L. CHU, H.T. HU and J.Y. WU. Dynamic response of a reinforced concrete slab subjected to air blast load. *Theoretical and Applied Fracture Mechanics*. 2011, vol. 56, issue. 3, pages.140–147. ISSN 0167-8442. DOI: 10.1016/j.tafmec.2011.11.002.

[6] ZHAO, C.F. and J.Y. CHEN. Damage mechanism and mode of square reinforced slab subjected to blast loading. *Theoretical and Applied Fracture Mechanics*. 2013, vol. 63-64, p. 54-62. ISSN 0167-8442. DOI: 10.1016/j.tafmec.2013.03.006.

[7] THIAGARAJAN, G., A.V. KADAMBI, S. ROBERT and C.F. JOHNSON. Experimental and finite element analysis of doubly reinforced concrete slabs subjected to blast loads. *International Journal of Impact Engineering*. 2015, vol. 75, p. 162-173. ISSN 0734-743X. DOI: 10.1016/j.ijimpeng.2014.07.018.

[8] DUBEC, B., P. MAŇAS, J. ŠTOLLER and P. STONIS. 2019. Experimental and numerical assessment of fibre reinforced concrete slab under blast load, *ICMT 2019 - 7th International Conference on Military Technologies, Proceedings* 2019. ISBN: 978-172814593-8. DOI: 10.1109/MILTECHS.2019.8870129.

[9] Livermore Software Technology Corporation (1997), LS-DYNA Theoretical Manual. Livermore, CA: Livermore Software Technology Corporation.

[10] SCHWER, L. E., Y. D. MURRAY. A three invariant smooth cap model with mixed hardening. *International Journal for Numerical and Analytical Methods in Geomechanics*, vol. 18, pp. 657-688, 1994. DOI: 10.1002/nag.1610181002.

[11] SANDLER, I. S., F. L. DIMAGGIO, G.Y. BALADI. Generalized cap model for geological materials, *ASCE Journal of the Geotechnical Division*, vol. 102, pp. 683-699, 1976.

[12] JIANG, H., J. ZHAO. Calibration of the continuous surface cap model for concrete, *Finite Elements in Analysis and Design*. 2015, vol. 97, p. 1-19. ISSN 0168-874X. DOI: 10.1016/j.finel.2014.12.002.

[13] ÚNMZ (2011), ČSN EN 1992-1-1 (73 1201) Eurokód 2: Navrhování betonových konstrukcí – Část 1-1: Obecná pravidla a pravidla pro pozemní stavby. Praha.

[14] MURRAY, Y. D., User's manual for LS-DYNA concrete material model 159, Report No. FHWA-HRT-05-062 Federal Highway Administration, 2007.

[15] MURRAY, Y. D., A. ABU-ODEH, R. BLIGH, Evaluation of concrete material model 159, Report No. FHWA-HRT-05-063, 2006.

[16] KRÁL, P., M. HUŠEK, P. HRADIL, J. KALA and P. MAŇAS, Optimization of the material parameters of the continuous surface cap model for concrete, 2017 *International Conference on Military Technologies* (ICMT), Brno, 2017, pp. 298–302. ISBN 978-1-5090-5666-8. DOI: 10.1109/MILTECHS.2017.7988773.

[17] JOHNSON G. R. and HOLMQUIST T. J. (1992). A computational constitutive model for brittle materials subjected to large strains, high strain rates and high pressures. In: *Shock wave and High-Strain-Rate Phenomena in Materials*, p. 1075-1081 edited by M.A. Meyers, L.E. Murr, and K.P. Staudhammer, New York: Marcel Dekker Inc., ISBN 0824785797.

[18] JINDRA, D., HRADIL, P. and KALA, J. (2020). Optimal adjustment of FE model of concrete slab exposed to impact loading. *MATEC Web Conf.* vol. 313 article no. 00024 (2020). DOI: 10.1051/matecconf/202031300024.

[19] RANDERS-PEHRSON, G. and K. A. BANNISTER. Airblast loading model for DYNA2D and DYNA3D. Army Research Laboratory, Rept. ARL-TR-1310, US, 1997.

[20] FRIEDLANDER, F. G. The diffraction of sound pulses I. Diffraction by a semi-infinite plane. *Proceedings of the Royal Society A*. 1946. ISSN 0080-5630. DOI: 10.1098/rspa.1946.0046.

[21] HOPKINSON, B., British Ordnance board minutes 13565, in: The National Archives, Kew, UK, 1915, pp.11.

[22] CRANZ, C., Lehrbuch der Ballistik. Erster Band. AusereBalistik, Springer Verlag, Berlin (1925).

[23] KARLOS, V., G. SOLOMOS. 2013. Calculation of blast loads for application to structural components. *JRC Technical Reports*, Report EUR 26456 EN, Luxembourg. ISSN 1831-9424. DOI:10.2788/61866.